15

Magnetic-pulse deformation of TiNi alloy: experiment and calculation

© E.S. Ostropiko, S.G. Magazinov, S.I. Krivosheev

Peter the Great Saint-Petersburg Polytechnic University,
St. Petersburg, Russia
e-mail: es-ostropiko@mail.ru, magazinov_sg@mail.ru, ksi.mgd@gmail.com

Received August 30, 2021
Revised October 6, 2021
Accepted October 7, 2021

Magnetic-pulse loading methods have been known since the 80s of the XX century and, as a rule, are used to determine the laws of destruction of materials under the action of pressure pulses with a duration of several microseconds. A modified scheme of a magnetic-pulse setup for high strain rate uniaxial tension is used in this work. The application of the scheme with the possibility of experimental measurement of the strain accumulation time and strain rate is shown on samples of TiNi alloy. The paper presents the results of finite element modeling and analytical description. Both approaches have demonstrated good agreement between the calculated residual strain and experimental results, even on samples of TiNi alloy with a specific stress-strain diagram. The analytical solution showed good qualitative agreement in assessing the strain accumulation time. On the basis of the analytical solution, an assessment of the capabilities of the magnetic-pulse loading method for uniaxial high strain rate tension is presented.

Keywords: magnetic-pulse loading, high strain rate deformation, TiNi alloy

DOI: 10.21883/0000000000

Introduction

Magnetic-pulse methods are used to generate controlled pressure pulses of a microsecond duration [1–3]. Methods of this class have been developed in the 1980s [4] and are often used to determine the laws of high-strain-rate destruction of materials [5,6]. They are specific in that a stress state is established without preloading, which may be important for materials with a spatial anisotropy of their strain characteristics (composites, layered materials, and certain metals) [7–10]. One of the schemes has been adapted earlier [11] to implement magnetic-pulse tension in the study of the properties of a TiNi shape-memory alloy after high-rate loading. It was demonstrated that this approach is suitable for high-strain-rate uniaxial tension studies of materials and may be used to examine their properties unrelated to destruction.

Shape-memory alloys have a set of unique features: high strength, corrosion resistance, biocompatibility, damping capacity, and, most importantly, shape recovery. When heated, they return partially or completely to their predetermined shape. The mechanism behind this is the thermoelastic reversible martensitic phase transition [12]. It is known that the functional properties of shape-memory alloys depend on the preloading pattern and the strain rate. The influence of strain rate on the mechanical properties and the structure of alloys [13–18], the pseudoelastic behavior [19–22], and the manifestation of functional properties [23–26] has been studied extensively. Almost all of these studies involve compression tests. The reason for this is obvious: the most widely used high-strain-rate deformation method is the Kolsky method [27]. Naturally, modifications of this method for tension tests were proposed [28], but they are rarely used, since they require specific preparation of samples and time-consuming processing of data that yields ambiguous results. Even in compression tests, the strain accumulation time is $100-200\,\mu$s, and the strain rate is usually below $1000-1500\,\mathrm{s}^{-1}$. It is almost impossible to find studies with higher strain rates in which the tested sample is not destroyed. One thing is beyond doubt: the question of influence of strain rate on the behavior of shape-memory alloys and metals in general attracts much research interest.

The aim of this study is to present a scheme of magnetic-pulse loading that was modified for uniaxial tension and allows for experimental measurement of the strain accumulation time, compare the experimental data (residual strain, strain accumulation time, strain rate) with the results of finite-element modeling and the analytical estimate for a TiNi alloy to verify their predictive capacity, perform analytical analysis of the loading scheme, and identify the probable trends.

1. Experimental procedure

The diagram of the experimental setup and the sizes of samples used in tests are presented in Fig. 1. The setup includes a pulsed current generator (PCG) and a pair of magnetic-pulse drivers (MPDs), which are flat copper buses 0.3 mm in thickness and 4 mm in width positioned in cutouts in the sample of a specific shape. C, L, R are the capacitance, the inductance, and the resistance of the generator and S is the discharge device. The generator produces current I due to the discharge of capacitor bank C.

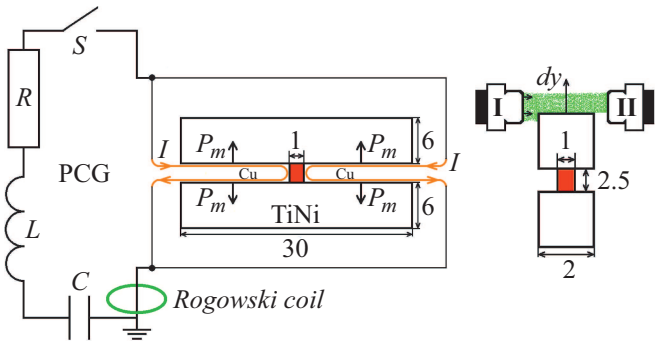

Figure 1. Diagram of the magnetic-pulse tension setup. Pulsed current generator with a TiNi alloy sample (left). Optical system for estimation of the strain accumulation time (right). I — laser, II — light guide. The working part of the sample and its dimensions are highlighted in red (online).

In the classical scheme, current flows through an MPD inserted into a cutout in the sample with a crack-type macrodefect [4]. In the scheme for uniaxial tension, current is distributed among two MPDs inserted symmetrically into the cutouts of a specially prepared sample. The space between the driver and the sample (as well as the space inside the driver loop) is filled with a dielectric material. A magnetic field is generated between the conduct buses of each MPD. Its parameters (shape, magnitude, duration) are defined uniquely by the current parameters. Magnetic pressure P_M affects the buses. It is applied symmetrically on either side of the working part of the sample to the edges of the cutout and induces uniaxial tension of the working part. Current pulse $I(t)$ is measured with the use of an oscilloscope and a Rogowski coil. The parameters of this coil are determined in accordance with the rules outlined in [29]. The PCG used in this study had charging voltage $U = 50\,\text{kV}$, capacitance $C = 14.8\,\mu\text{F}$, and inductance $L = 80\,\text{nH}$.

The displacement rate of the sample was measured using a laser technique based on measuring the intensity of laser radiation with the sample end (edge) crossing the optical path. The laser, which was directed at the end face of the sample, was connected via a converter to an oscilloscope. A light guide was located behind the sample. When the sample is deformed, its end face moves, blocks the path to the light guide, the flux intensity decreases, and the signal amplitude at the oscilloscope also decreases.

We made an attempt to record the test on a high-speed camera (Photron FASTCAM SA5). The record confirmed the assumption of symmerical displacement of sample non-working parts under a pressure pulse. This effect was observed in tension to a specified residual strain and was preserved up to the moment of destruction of the sample. The symmetric nature of deformation motivated the choice of the laser technique.

The parameters of a current pulse (frequency and damping coefficient) could be adjusted by varying the PCG parameters. The pulse amplitude could be varied by altering the capacitor charge. In our tests, the pulse was a damped sinusoid with a ratio of neighboring amplitudes of ~ 0.6 and a period of $6-7\,\mu$s (Fig. 2, *a*).

The magnetic pressure (Fig. 2, *b*) is determined in accordance with the following formula [4,5]:

$$P_m = k\frac{\mu}{2}\left(\frac{I}{b}\right)^2, \tag{1}$$

where $\mu = 4\pi 10^{-7}\,\text{H/m}$ is the magnetic constant, I is the current flowing through a conductor, b is the conductor width, and k is the coefficient of correction for the driver geometry and the fact that the current distribution over the width of driver buses becomes nonuniform at higher frequencies. In the case under study, $k \approx 0.42$ [5].

Samples were cut by electrical discharge machining from a plate with a thickness of 2 mm. The section area of the working part was $1\,\text{mm}^2$, and the height was 2.5 mm. The height of non-working parts was 6 mm, and the length was 30 mm. The mass of samples was $\sim 5\,\text{g}$. These samples preserved the symmetry and parallelism of non-working parts in all tests (even in those resulting in destruction): the non-working parts remained almost undeformed under the influence of magnetic pressure, and strain was accumulated in the working part.

2. Analytical estimate and finite-element modeling

An analytical description of the deformation process in the considered loading scheme was proposed earlier in [30]. We use the same approach, but apply it to determine the residual strain (with unloading taking into account) instead of the maximum accumulated strain. It should be noted that this solution is valid only for samples with undeformed non-working parts (i.e., when the entire pulse is focused on deforming the working part). With this assumption and the symmetry of the problem taken into account, the equation of motion assumes the form

$$m\ddot{y}(t) = F(t) - S_0\sigma(t), \tag{2}$$

where m is the mass of one half of the sample, S_0 is the section area of the working part, and $\sigma(t)$ is the stress in the working part of the sample under tension (Fig. 3, *a*).

External force $F(t)$ is defined in terms of magnetic pressure $P_M(t)$, which is related to current pulse

$$F(t) = SP_M(t) = SP\frac{\sin^2(2\pi f t)}{e^{2t/\tau}}, \tag{3}$$

where f is frequency, τ is the damping time constant, S is the area of application of magnetic pressure, and P is a parameter chosen so as to match the amplitude value with the experimental one (Fig. 3, *b*). Since nonlinear elements are present in the PCG circuit (e.g., a spark discharger and current-carrying elements that are heated by the passage of

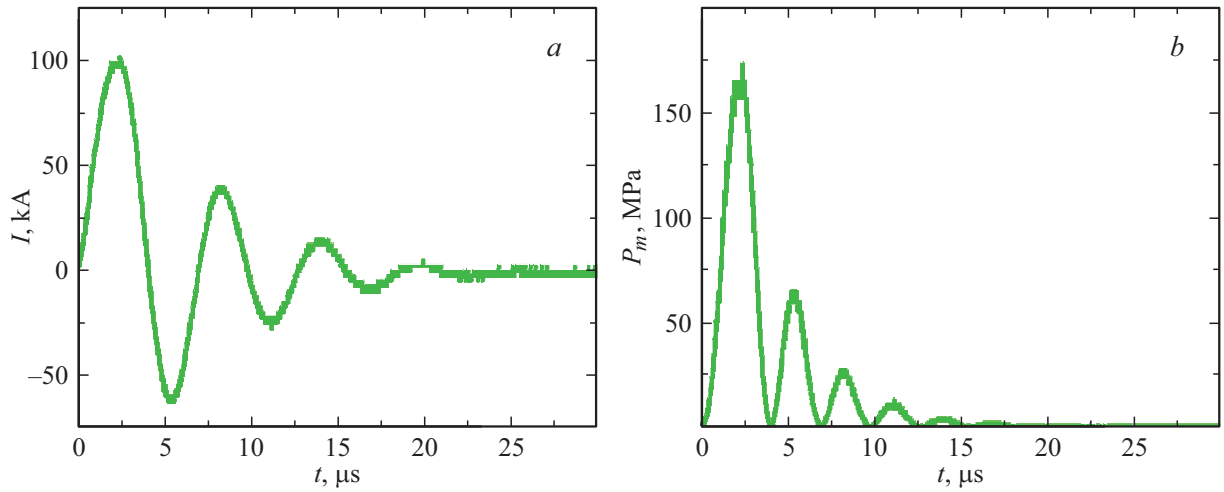

Figure 2. Example oscilloscope record of current pulse $I(t)$ (a) and the corresponding magnetic pressure $P_M(t)$ (b). Taken from the test to a residual strain of $\sim$ 15%.

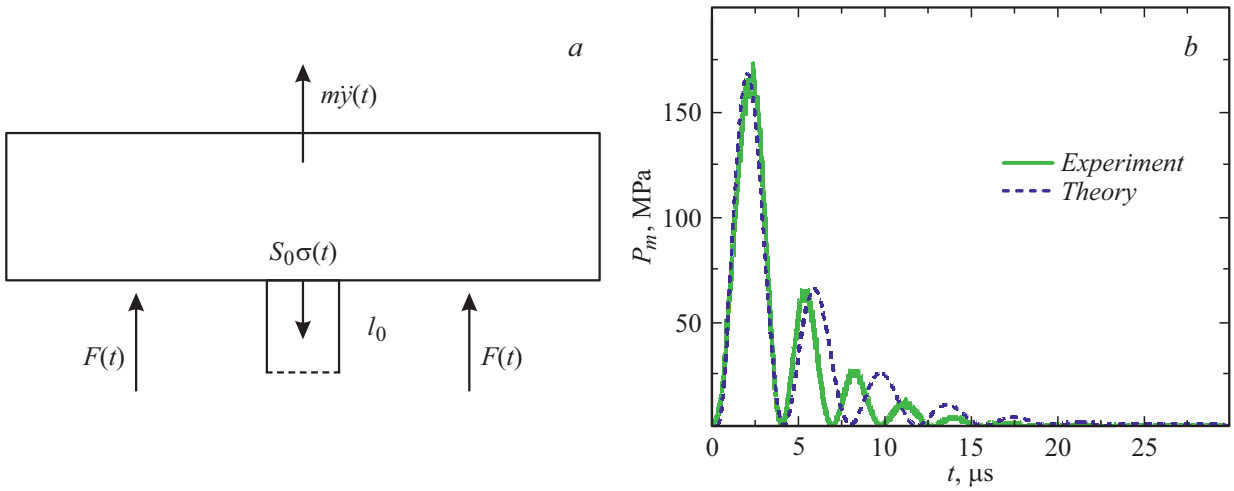

Figure 3. Diagram of the problem (a). Experimental magnetic pressure pulse and its theoretical approximation (b). Taken from the test to a residual strain of $\sim$ 15%.

current), the shape of the current (pressure) pulse differs somewhat from an ideal damped sinusoid. Therefore, in order to compare the experimental and calculated data, the parameters of external influence were chosen so as to ensure the maximum similarity for the first two peaks of the pressure pulse (the most energy-intensive and efficient ones).

The strength of material is defined in the piecewise-linear approximation by a set of equations of straight lines based on the stress–strain curve of the material under study (Fig. 4):

$$\sigma(t) = a\varepsilon(t) + b = a\,\frac{y(t)}{l_0} + b, \qquad (4)$$

where l_0 is the initial length of the working part of the sample; a, b are parameters of straight sections of the piecewise-linear approximation that are easy to determine from the boundaries of these sections. The stress–strain diagram was obtained using a multipurpose test machine fitted with a videoextensometer. The structural behavior of shape-memory materials in the low-temperature martensitic phase is unordinary: following an elastic section, these materials undergo, upon reaching the reorientation limit local plastic deformation due to martensite reorientation. The remaining sections of the curve are ordinary: a proportional section of deformation of the reoriented structure is followed, upon reaching the yield point, by dislocation plastic deformation. Naturally, the loading rate affects the reorientation, yield, and ultimate stress limits of a material: the higher the rate, the higher these limits [26,31]. However, this influence does not translate into a critical difference and may be neglected in theoretical estimation of the behavior of a material.

A series of tests with unloading was performed in addition to tension tests. These sections may also be approximated with segments parallel to each other. This

allows one to determine the strain relief law. Coordinates of the vertices of the piecewise-linear approximation are as follows: (0;0), (0.5;160), (5.2;180), (11.2;750), (50;1150).

The general solution of (2) with (3) and (4) taken into account has the following form:

$$y(t) = C_1 \sin\sqrt{A}t + C_2 \cos\sqrt{A}t - \frac{B}{A} + \frac{F\tau^2}{2A\tau^2+8} e^{-\frac{2t}{\tau}} + \frac{8F\pi f\tau^3}{(4+A\tau^2-16\pi^2 f^2\tau^2)^2+256\pi^2 f^2\tau^2} e^{-\frac{2t}{\tau}} \sin 4\pi f t + \frac{8F\pi^2 f^2\tau^4 - 2F\tau^2 - \frac{FA\tau^4}{2}}{(4+A\tau^2-16\pi^2 f^2\tau^2)^2+256\pi^2 f^2\tau^2} e^{-\frac{2t}{\tau}} \cos 4\pi f t, \quad (5)$$

where $A = S_0 a/ml_0$, $B = S_0 b/m$, $F = SP/m$.

We determine C_1 and C_2 presuming that $y(0) = 0$, $\dot{y}(0) = 0$ at the initial time, and the initial conditions at a certain section should correspond to the values achieved at the end of the previous section. The time dependences of displacement are achieved after solving the Cauchy problems at sections of the piecewise-linear approximation. The overall displacement is then obtained by summing up the $y(t)$ increments at each section into a common sequence. Ratio $\varepsilon(t) = y(t)/l_0$ characterizes the temporal variation of strain. The maximum of this ratio corresponds, first, to the moment of accumulation of the maximum strain and, second, to the moment when linear relief commences in accordance with the unloading rule.

Finite-element modeling of the material behavior under magnetic-pulse loading was performed in ANSYS Workbench. The mechanical material properties used in this modeling were as follows: TiNi density — 6500 kg/m^3, Young's modulus — 32 GPa, Poisson ratio — 0.33. Nonlinear plasticity was defined in a similar way: as a piecewise-linear approximation of the stress–strain diagram in accordance with Fig. 4.

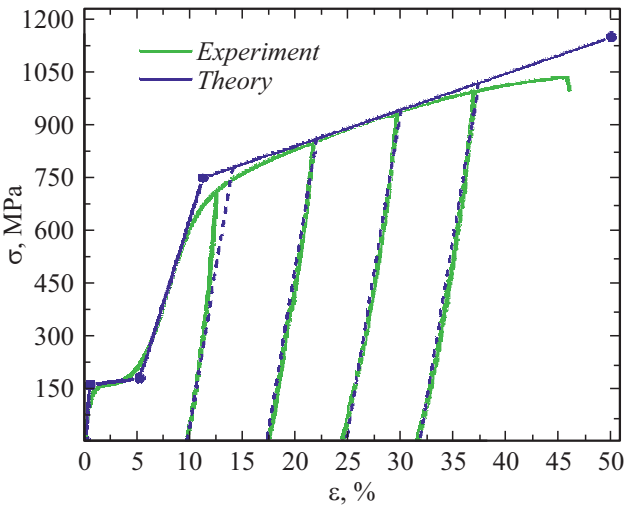

Figure 4. Stress–strain curve for the TiNi alloy and its piecewise-linear approximation. Vertices of the piecewise-linear approximation: (0;0), (0.5;160), (5.2;180), (11.2;750), (50;1150).

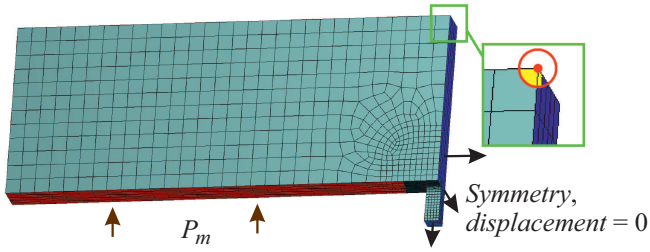

Figure 5. Configuration of the finite-element mesh and the studied node.

Since the problem is symmetric, a part of the sample was used for modeling with the symmetry and displacement conditions added to the corresponding surfaces (Fig. 5).

A magnetic pressure pulse from the experiment was used as loading pulse P_m. The strain and the strain accumulation time were estimated based on the displacement of the node highlighted in Fig. 5.

3. Calculation results and comparison with the experiment

Having performed a series of tests, we obtained a set of experimental values and dependences: mass of the sample, its geometric parameters, current pulse $I(t)$, and the dependence characterizing the variation of light intensity with time $U(t)$, which is related to the displacement of the sample end under load. The amplitudes of magnetic pressure were derived from $I(t)$ amplitudes using (1): 160, 173, 200, 260 MPa. Varying parameters P, f, τ for (3), we obtained an analytical approximation of loading pulses in each individual test (see Fig. 3, *b*). Having inserted all parameters (mass m, working part section S_0, loading surface area S, initial length l_0 of the working part, parameters a and b of piecewise-linear sections, pulse parameters P, f, τ) into (5) and formed a common sequence of the $y(t)$ increments, we obtained the time dependences of strain $\varepsilon(t) = y(t)/l_0$. With the amplitude value of $\varepsilon(t)$ known, we managed to determine the residual strain in linear approximation (4) in accordance with the strain relief rule and Fig. 4.

The results of finite-element modeling in ANSYS are presented in the form of a $y(t)$ dependence for the node highlighted in Fig. 5. A finite-element time dependence of strain $\varepsilon(t) = y(t)/l_0$ was plotted in a similar way.

Figure 6 presents the resulting $\varepsilon(t)$ dependences obtained in analytical calculations and finite-element modeling and the $U(t)$ dependence, which characterizes the temporal variation of light intensity with displacement of the sample end, for the sample deformed to a residual strain of $\sim 16\%$.

The noise seen in the experimental $U(t)$ dependence at the start of testing is attributable to the discharger operation. When the sample starts to deform, it blocks the light guide, the intensity decreases, and the oscilloscope voltage drops from ~ 3.1 to ~ 2.4 V. This is the reason why the scale

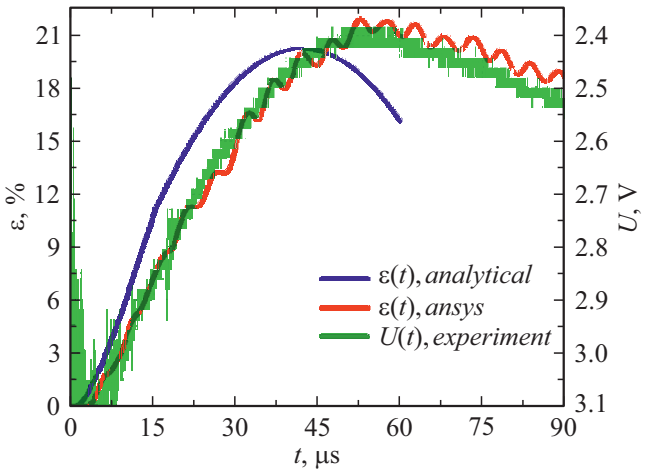

Figure 6. $\varepsilon(t)$ dependences obtained in analytical calculations and finite-element modeling. Dependence $U(t)$ characterizes the temporal variation of intensity of the light beam. Taken from the test to a residual strain of $\sim 16\%$.

is inverted. It can be seen that all three curves agree qualitatively at the strain accumulation stage. The maximum strain values in calculated dependences are close, although the finite-element value is somewhat higher than the one provided by analytical calculations. The wave nature of deformation is taken into account in the ANSYS calculation. The $\varepsilon(t)$ curve demonstrates this clearly: owing to its wave nature with periodic strain „dips," the strain accumulation time t_m is longer than that in the analytical calculation. This makes the ANSYS curve qualitatively closer to the experimental one. The wave nature is not taken into account in analytical calculations, and strain is thus accumulated faster.

Figure 7 presents the experimental and calculated dependences of residual strain ε_{res}, strain accumulation time t_m, and plastic strain rate $\dot{\varepsilon} = \varepsilon_{res}/t_m$ on amplitude P_m of the magnetic pressure.

The calculated residual strain values agree with the experimental ones (Fig. 7, *a*). However, the ANSYS values

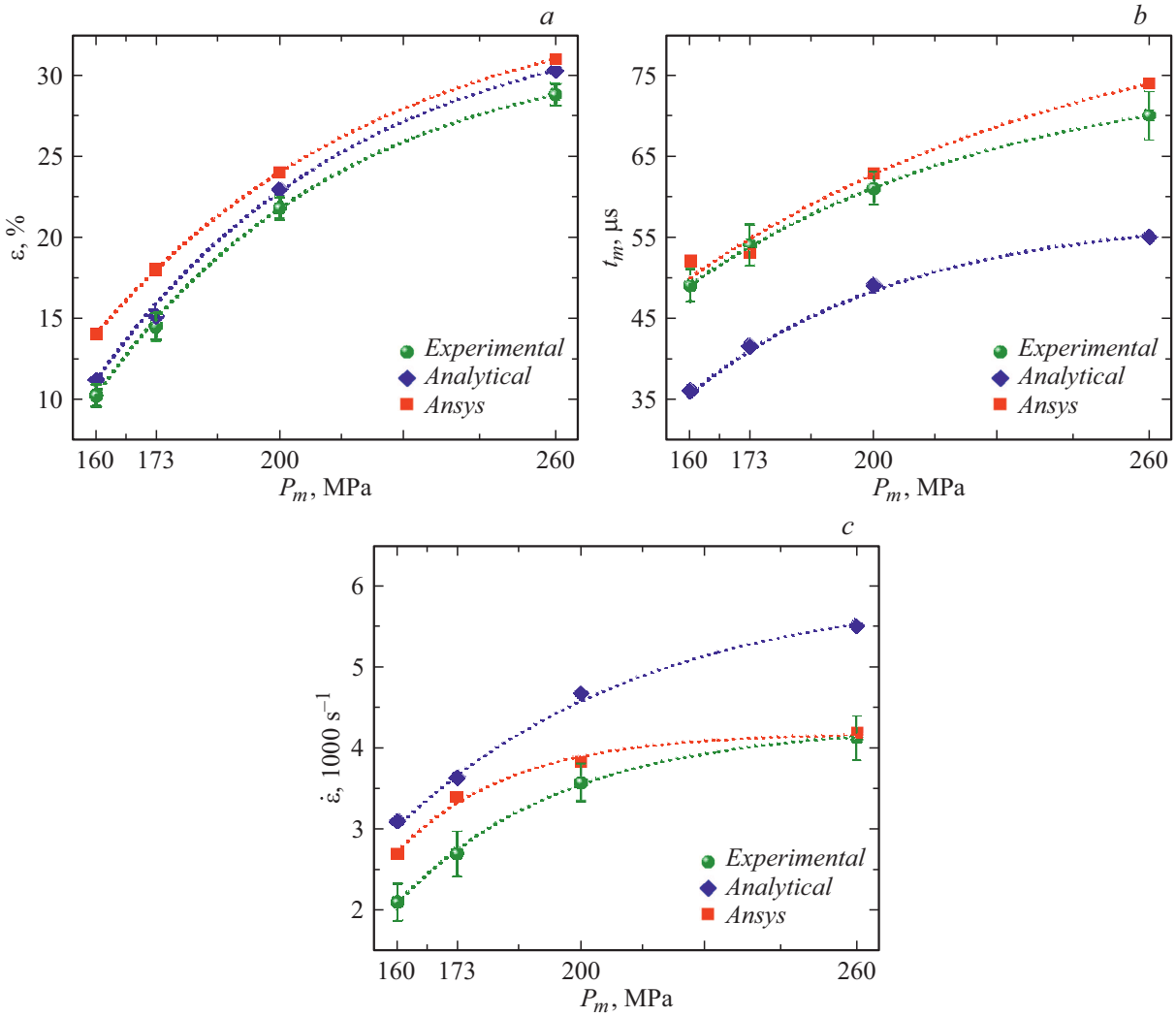

Figure 7. Experimental and calculated dependences of residual strain ε_{res} (*a*), strain accumulation time t_m (*b*), and plastic strain rate $\dot{\varepsilon}$ (*c*) on amplitude P_m of the magnetic pressure.

of residual strain are somewhat higher than the experimental ones (especially in low-strain tests). Apparently, this is attributable to the specifics of calculations in the martensite reorientation region. The observed difference is smoothed out at higher strain values: the higher the strain, the smaller the contribution of this section to the overall calculated strain and the closer the calculated values to the experimental ones. Thus, at higher strain values, ANSYS provides a more accurate representation of the experiment in terms of all the studied parameters.

The analytical estimates of strain accumulation time t_m (Fig. 7, b) are 20–30% lower than the experimental ones. However, the curves agree qualitatively. ANSYS provides more accurate values with a difference of just 5–10%. As a result, the $\dot{\varepsilon}$ dependence features a similar set of differences, since $\dot{\varepsilon} = \varepsilon_{res}/t_m$. It can be seen from Fig. 7, c that the analytical estimates of plastic strain rate are, on the average, 35–40% higher than the experimental values, but a qualitative agreement is preserved. ANSYS provides $\dot{\varepsilon}$ values that are closer to the experimental ones in the considered test range, but the obtained dependences differ qualitatively. At small amplitudes of the pressure pulse, the average ANSYS plastic strain rate values are closer to the analytical ones; at high pulse amplitudes, they approach the experimental values.

It is fair to say that both methods provide a reasonable agreement between the calculated residual strain and the experimental data for initial estimation. ANSYS is more accurate in estimating the strain accumulation time, but the analytical method, while being simpler and easier to implement, also provides a qualitatively correct representation of the material behavior.

Drawing on the obtained qualitative agreement and the predictive capacity of the analytical solution, we performed a series of calculations on the deformation of similar samples (Fig. 1) by pulses of a similar shape (Fig. 2). For convenience, we set $\varepsilon = 50\%$ as the limit strain and analyze the variation of accumulation time t_m of this strain with the loading pulse frequency and the sample mass (Fig. 8, a). Mass $m = 5$ g corresponds to the mass of the experimental sample. Curve $T/2$ in Fig. 8, a represents one half of a period of the pulse of the corresponding frequency.

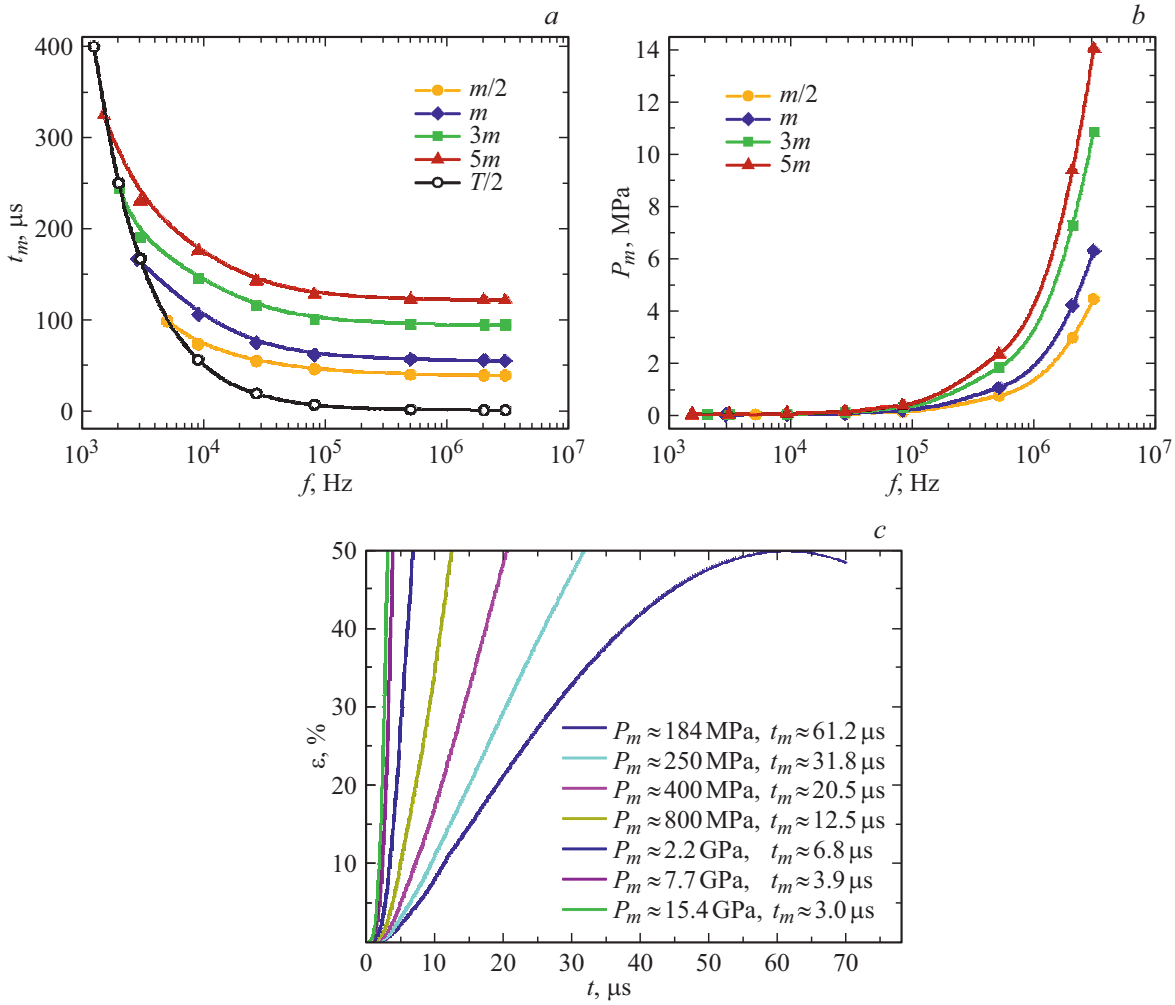

Figure 8. Results of analytical calculations. Mass $m = 5$ g. Time of accumulation of 50% strain as function of the sample mass and the loading pulse frequency (a) and the corresponding amplitude P_m of the magnetic pressure (b). $\varepsilon(t)$ dependences for pulses of different amplitudes with a frequency of 80 kHz (c).

As expected, the $t_m(f)$ curve shifts downward as the sample mass decreases, since the sample becomes less inertial. At low frequencies of the loading pulse, time t_m becomes comparable to $T/2$; i.e., the deformation process becomes quasistatic. As the pulse frequency increases, time t_m tends asymptotically to a certain value. Therefore, the set strain level is characterized by a certain minimum possible strain accumulation time that is defined by the period of natural vibrations of the considered sample.

No appreciable reduction in t_m is seen at frequencies above $f = 80$ kHz. However, a significant increase in amplitude P_m is needed at high frequencies to accumulate the corresponding strain (Fig. 8, *b*). Technically, it can be said that the frequency range of 80–150 kHz is the optimum one for the studied material, since almost minimum t_m values are achieved here without the need for extreme magnetic pressures.

Naturally, if a destruction test needs to be performed, an increased amplitude P_m will result in faster accumulation of the same $\varepsilon = 50\%$ and destruction. Figure 8, *c* presents the $\varepsilon(t)$ dependences for pulses of different amplitudes with a frequency of 80 kHz ($T = 12.5\,\mu$s). It can be seen that accumulation time t_m become comparable to the period of the loading pulse as P_m increases. The pressure amplitude limits for the considered loading method are associated with the magnetic field induction (its maximum possible amplitude is related to the sublimation energy of the material of the magnetic system) and parameters of the pulsed current generator. It was demonstrated in [32] that the maximum magnetic field induction in a copper magnetic system is 340–360 T. The magnetic pressure may reach a level of 50 GPa.

The pulse frequency in the experiments was ≈ 140 kHz. The maximum achieved residual strain was $\approx 29\%$, and its accumulation time was $\approx 68\,\mu$s; i.e., the plastic strain rate was $\approx 4300\,\text{s}^{-1}$. The above suggests that these are the nearly maximum values of strain accumulation time and strain rate for the considered loading scheme in tests that should not result in the destruction of samples. The strain rate may be increased by reducing the sample mass.

Naturally, this analytical estimation method is applicable not just to the TiNi alloy, but to any metal with a known stress–strain diagram.

Conclusion

The application of magnetic-pulse loading in uniaxial tension tests with experimental measurement of the strain accumulation time was demonstrated using the example of TiNi alloy samples.

Analytical and finite-element calculations of the residual strain, the strain accumulation time, and the strain rate were performed. The residual strain estimates calculated using both approaches agree quantitatively with the experimental values (even for TiNi alloy samples with a nonconventional stress–strain diagram). The agreement is sufficient for these data to be used to design experiments.

The finite-element ANSYS simulation software provides more accurate estimates of the strain accumulation time in the considered test range (especially at high strain values). However, when it comes to the qualitative material behavior, the analytical solution is better in characterizing the dependence of the average plastic strain rate on the magnetic pressure amplitude.

It was demonstrated theoretically that loading with pulses with frequencies above 80–150 kHz is impractical, since a considerable increase in the magnetic pressure amplitude is needed to achieve the corresponding strain values, but the gain in strain accumulation time is almost nonexistent. It is more practical to reduce the sample size or alter the design of the loading system.

It follows from the results of calculations that the set strain level in the considered loading scheme (sample–loading scheme–PCG) is characterized by a certain minimum possible strain accumulation time that is defined by the period of natural vibrations of the considered sample. The sample mass needs to be reduced in order to reduce the time needed to achieve the required strain. If a destruction test needs to be performed, an increased amplitude will result in faster accumulation of ultimate strain and destruction. The magnetic pressure amplitude is limited only by the magnetic field induction (its maximum is related to the sublimation energy of the material of the loading system) and parameters of the pulsed current generator.

Acknowledgments

Finite-element modeling in ANSYS was performed using the computational resources of the supercomputing center of Peter the Great St. Petersburg Polytechnic University.

Funding

This study was supported financially by the Russian Foundation for Basic Research (project No. 19-32-60035).

Conflict of interest

The authors declare that they have no conflict of interest.

References

[1] D.I. Alekseev, S. I. Krivosheev, S.G. Magazinov. MATEC Web Conf., **145**, 05006, (2018). DOI: 10.1051/matecconf/201814505006

[2] H. Ma, W. Mao, H.l. Su, H. Zhu, X. Cui, L. Huang, J. Li, M. Wu. Int. J. Mech. Sci., **209**, 106712 (2021). DOI: 10.1016/j.ijmecsci.2021.106712

[3] A. Gruzdkov, S. Krivosheev, Yu. Petrov, A. Razov, A. Utkin. Mater. Sci. Eng. A, **481**–**482**, 105 (2008). DOI: 10.1016/j.msea.2007.03.113

[4] K.R. Chandar, W.G. Knauss. Int. J. Fract., **20**, 209 (1982). DOI: doi.org/10.1007/BF01140336
[5] S.G. Magazinov, S.I. Krivosheev, Yu.E. Adamyan, D.I. Alekseev, V.V. Titkov, L.V. Chernenkaya. Mater. Phys. Mech., **40**, 117 (2018). DOI: 10.18720/MPM.4012018_14
[6] S. Atroshenko, V. Morozov, D. Gribanov, A. Lukin, Y. Petrov. EPJ Web Conf., **94**, 02014 (2015). DOI: 10.1051/epjconf/20159402014
[7] G.I. Kanel, S.V. Razorenov, V.E. Fortov. Joint 20th AIRAPT — 43th EHPRG (Karlsruhe, Germany, 2005), 119921.
[8] G.I. Kanel, S.V. Razorenov, G.V. Garkushin, A.S. Savinykh. J. Phys. Conf. Ser., **946**, 012039 (2018). DOI: 10.1088/1742-6596/946/1/012039
[9] Y. Meshcheryakov, A. Divakov, N. Zhigacheva, G. Konovalov. Proc. Struct. Int., **2**, 477 (2016). DOI: 10.1016/j.prostr.2016.06.062
[10] G.G. Savenkov, Yu.I. Meshcheryakov, B.K. Barakhtin, N.V. Lebedeva. J. Appl. Mech. Tech. Phys., **55**, 896 (2014). DOI: 10.1134/S0021894414050198
[11] E.S. Ostropiko, S.I. Krivosheev, S.G. Magazinov. Appl. Phys. A, **127**, 27 (2021). DOI: 10.1007/s00339-020-04160-7
[12] K. Otsuka, X. Ren. Progr. Mater. Sci., **50**, 511 (2005). DOI: 10.1016/j.pmatsci.2004.10.001
[13] V. Grigorieva, A. Danilov, A. Razov. Acta Phys. Pol., **128**, 592 (2015). DOI: 10.12693/APhysPolA.128.592
[14] S.-Y. Jiang, Y.-Q. Zhang. Trans. Nonferrous Met. Soc. China., **22** (1), 90 (2012). DOI: 10.1016/S1003-6326(11)61145-X
[15] S.-Y. Jiang, Y.-Q. Zhang, Y.-N. Zhao, M. Tang, W.-L. Yi. J. Cent. South Univ., **20**, 24 (2013). DOI: 10.1007/s11771-013-1454-6
[16] A.M. Bragov, L.A. Igumnov, A.Yu. Konstantinov, A.K. Lomunov, A.I. Razov. Adv. Struct. Mater., **103**, 133 (2019). DOI: 10.1007/978-3-030-11665-1
[17] Y. Qiu, M.L. Young, X. Nie. Metall. Mater. Trans. A, **46**, 4661 (2015). DOI: 10.1007/s11661-015-3063-5
[18] Y. Qiu, M.L. Young, X. Nie. Metall. Mater. Trans. A, **48**, 601 (2017). DOI: 10.1007/s11661-016-3857-0
[19] W.W. Chen, Q. Wu, J.H. Kang, N.A. Winfree. Int. J. Solids Struct., **38** (50−51), 8989 (2001). DOI: 10.1016/S0020-7683(01)00165-2
[20] S. Nemat-Nasser, W.-G. Guo. Mech. Mater., **38**, 463 (2006). DOI: 10.1016/j.mechmat.2005.07.004
[21] H. Tobushi, Y. Shimeno, T. Hachisuka, K. Tanaka. Mech. Mater., **30** (2), 141 (1998) DOI: 10.1016/S0167-6636(98)00041-6
[22] J. Zurbitu, R. Santamarta, C. Picornell, W.M. Gan, H.-G. Brokmeier, J. Aurrekoetxea. Mat. Sc. Eng. A., **528** (2), 764 (2010). DOI: 10.1016/j.msea.2010.09.094
[23] V.A Likhachev, Yu.I. Patrikeev, in *Tezisy dokladov XXIV vsesoyuznogo seminara „Aktual'nye problemy prochnosti,"posvyashchennogo mekhanike prochnosti materialov s novymi funktsional'nymi svoistvami* (Rubezhnoe, SSSR, 1990), p. 128 (in Russian).
[24] S.P. Belyaev, N.F. Morozov, A.I. Razov, A.E. Volkov, L.L. Wang, S.Q. Shi, S. Gan, J. Chen, X.L. Dong. Mater Sci Forum., **394**−**395**, 337 (2002). DOI: 10.4028/www.scientific.net/MSF.394-395.337
[25] E.S. Ostropiko, A.Y. Konstantinov. Lett. Mater., **11** (2), 223 (2021). DOI: 10.22226/2410-3535-2021-2-223-228
[26] E.S. Ostropiko, A.Y. Konstantinov. Mater. Sci. Technol., **37** (4), 1 (2021). DOI: 10.1080/02670836.2021.1958466
[27] H. Kolsky. Proc. Phys. Soc. London Sect. B., **62** (11), 676 (2002). DOI: 10.1088/0370-1301/62/11/302
[28] T. Nicholas. Exp. Mech., **21** (5), 177 (1981). DOI: 10.1007/BF02326644
[29] H. Knoepfel, *Pulsed High Magnetic Fields: Physical Effects and Generation Methods Concerning Pulsed Fields Up to the Megaoersted Level* (North-Holland, 1970).
[30] E.S. Ostropiko, S.I. Krivosheev, S.G. Magazinov. Lett. Mater., **11** (1), 55 (2021). DOI: 10.22226/2410-3535-2021-1-55-60
[31] A.M. Bragov, A.N. Danilov, A.Yu. Konstantinov, A.K. Lomunov, A.S. Motorin, A.I. Razov. Phys. Met. Metallogr., **116** (4), 385 (2015). DOI: 10.1134/S0031918X15040031
[32] S.I. Krivosheev. Digest Technical Papers — IEEE International Pulsed Power Conf., **2**, 750 (1999). DOI: 10.1109/PPC.1999.823622